A Droplet-Based Microfluidic Platform for High-Throughput, Multi-Parameter Screening of Photosensitizer Activity.

ARTICLE *in* ANALYTICAL CHEMISTRY · AUGUST 2013

Impact Factor: 5.64 · DOI: 10.1021/ac4022067 · Source: PubMed

11 AUTHORS, INCLUDING:

Dong-Ku Kang
University of California, Irvine
34 PUBLICATIONS **630** CITATIONS
SEE PROFILE

Xize Niu
University of Southampton
47 PUBLICATIONS **1,280** CITATIONS
SEE PROFILE

Soo-Ik Chang
Chungbuk National University
91 PUBLICATIONS **1,654** CITATIONS
SEE PROFILE

Robert C R Wootton
ETH Zurich
35 PUBLICATIONS **960** CITATIONS
SEE PROFILE

analytical chemistry

Article

pubs.acs.org/ac

Droplet-Based Microfluidic Platform for High-Throughput, Multi-Parameter Screening of Photosensitizer Activity

Soongwon Cho,[†] Dong-Ku Kang,[†] Steven Sim,[†] Florian Geier,[‡] Jin-Young Kim,[§] Xize Niu,[⊥] Joshua B. Edel,[†] Soo-Ik Chang,[¶] Robert C. R. Wootton,[∥] Katherine S. Elvira,*[,∥] and Andrew J. deMello*[,∥]

[†]Department of Chemistry, Imperial College London, South Kensington Campus, London SW7 2AZ, United Kingdom

[‡]Department of Surgery and Cancer, Faculty of Medicine, South Kensington Campus, Imperial College London, London, SW7 2AZ, United Kingdom

[§]Department of Bioengineering, South Kensington Campus, Imperial College London, London, SW7 2AZ, United Kingdom

[⊥]Engineering and the Environment, and Institute for Life Sciences, University of Southampton, Highfield, Southampton, SO17 1BJ, United Kingdom

[¶]Department of Biochemistry, Chungbuk National University, Cheongju, Chungbuk, Korea

[∥]Institute for Chemical and Bioengineering, Department of Chemistry and Applied Biosciences, ETH Zürich, Wolfgang-Pauli-Strasse 10, CH-8093 Zürich, Switzerland

Supporting Information

ABSTRACT: We present a fully integrated droplet-based microfluidic platform for the high-throughput assessment of photodynamic therapy photosensitizer (PDT) efficacy on *Escherichia coli*. The described platform is able to controllably encapsulate cells and photosensitizer within pL-volume droplets, incubate the droplets over the course of several days, add predetermined concentrations of viability assay agents, expose droplets to varying doses of electromagnetic radiation, and detect both live and dead cells online to score cell viability. The viability of cells after encapsulation and incubation is assessed in a direct fashion, and the viability scoring method is compared to model live/dead systems for calibration. Final results are validated against conventional colony forming unit assays. In addition, we show that the platform can be used to perform concurrent measurements of light and dark toxicity of the PDT agents and that the platform allows simultaneous measurement of experimental parameters that include dark toxicity, photosensitizer concentration, light dose, and oxygenation levels for the development and testing of PDT agents.

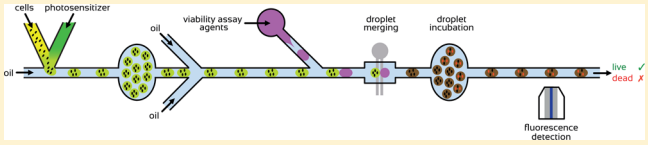

It is widely recognized that conventional antimicrobial treatments are becoming increasingly ineffective due to the emergence of multidrug resistant bacterial strains.[1−4] Photodynamic therapy (PDT) represents an efficacious modality for the treatment of localized microbial infections with a broad spectrum of action, efficient inactivation of multidrug-resistant bacteria, and low mutagenic potential.[5] More specifically, PDT is ideally suited for the treatment of multidrug resistant microbial infections since pathogens cannot readily develop resistance to PDT.[1] Additionally, PDT can be targeted for the treatment of localized infections. Various parameters such as photosensitizer concentration, light dose, and dissolved oxygen concentration must be examined to fully characterize the photodynamic inactivation process.[6,7] This is due to the fact that oxygen often plays a central role in the mechanism of the photodynamic inactivation, since the excited photosensitizer reacts with molecular oxygen to produce highly cytotoxic singlet oxygen species.[8] The general mechanism of action of these sensitizers is shown in Figure S1 in the Supporting Information. Understanding which inactivation pathway dominates in a particular sensitizer/pathogen system is vital in predicting the potential efficacy of the sensitizer. Unfortunately, conventional cytotoxicity screening of photosensitizers against microbial organisms is slow and laborious, requiring extensive culture comparison after incubation periods of over 18 h.[9] Accordingly, it is difficult to screen multiple parameters such as photosensitizer concentration, light dose, and the effect of poor oxygen supply in a high-throughput manner. Indeed, without rapid methods for screening photosensitizer toxicity, structure−activity relationships cannot be easily assessed.

Droplet-based (or segmented flow) microfluidic technology has recently emerged as a promising platform for performing high-throughput toxicity screening.[10−13] The ability to generate and manipulate pL-volume droplets at frequencies in excess of 1 kHz offers a direct route to ultrahigh analytical throughput combined with reduced reagent consumption, facile integration of various functional components, and rapid analysis.[14,15] Importantly, since the droplets are encapsulated by an immiscible continuous phase, cross-contamination between

Received: July 18, 2013
Accepted: August 12, 2013
Published: August 12, 2013

   dx.doi.org/10.1021/ac4022067 | *Anal. Chem.* 2013, 85, 8866−8872

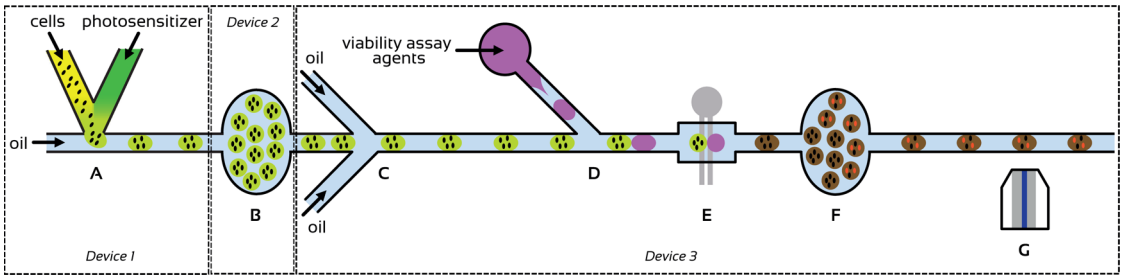

Figure 1. Schematic of the three microfluidic devices that form the droplet-based microfluidic photosensitizer screening platform. Device 1 is used for droplet generation. (A) *E. coli* cells and photosensitizer are encapsulated into droplets in a fluorinated oil continuous phase. Device 2 is used for droplet incubation. (B) Droplets are collected in a TPE chamber in Device 2 and incubated under both dark and light conditions. Device 3 is used for viability scoring assays. (C) After incubation, droplets are reinjected from the storage chamber into the viability scoring device and extra oil is injected via side channels to regulate the space between the droplets. (D) Droplets containing agents for the viability assay are created and interspersed with the droplets containing *E. coli*. (E) Electrofusion is used to merge droplets containing *E. coli* and the viability assay mixture. (F) Fused droplets are then incubated, in this case within a delay line consisting of a large PDMS channel, for 25 min before fluorescence detection (G).

sample droplets is minimized, as is interaction of the contained analytes with the channel walls.[16] Furthermore, since droplets contained within a segmented flow can be made to move at uniform velocity, Taylor dispersion is removed and the control of reaction (or residence) times is both precise and simple. Not surprisingly, a variety of basic droplet operations have been demonstrated using both active and passive approaches. These include droplet coalescence,[17−21] compartmentalization of chemically separated components,[22,23] mixing of droplet contents,[24,25] direct delivery of analytes into droplets,[26] droplet incubation,[27,28] droplet sorting,[29−31] and droplet dilution.[32]

Droplet-based microfluidic devices are most commonly manufactured from polydimethylsiloxane (PDMS) using well-explored soft lithography protocols.[33] Other substrate materials have also been used to make microfluidic devices for droplet manipulations. These include glass, silicon, and thermoset polyester (TPE).[22,34,35] Of these, TPE is of special interest because it has strong ultraviolet (UV) absorption, high transmission of visible light (over 80% transmittance at 600 nm), a large Young's modulus and can withstand pressures of up to 17.8 MPa (compared to 1.2 MPa for PDMS).[22] It is therefore ideal for the fabrication of microfluidic devices capable of droplet collection and reinjection under high pressures and allowing efficient light transmission over a wide range of wavelengths.

In recent years, a number of droplet-based microfluidic systems have been shown to be of potential utility in high-throughput screening applications, exhibiting improved efficiency and functionality compared to conventional screening systems.[10,12,36−39] For example, in the context of cytotoxicity screening in hospital environments, droplet-based microfluidic systems are attractive since they require small sample volumes for analysis and can rapidly produce patient-specific antimicrobial photosensitizer dose-response graphs without the need for incubation of bacterial cells for extended periods of time.[11] To this end, and given the multifactorial nature of photosensitizer activity and the relatively low-throughput offered by standard colony forming unit (CFU) assays, we sought to develop a high-throughput approach that relies on direct readout of cell viability. Accordingly, we present a modular, droplet-based microfluidic platform for performing high-throughput cytotoxicity screening of photosensitizing conditions against *Escherichia coli* (*E. coli*). The microfluidic system is able to screen a range of experimental parameters that impact cell cytotoxicity in high-throughput, using extremely small quantities (4.5 μL per assay point) of reagents. Significantly, the platform integrates multiple operations including cell encapsulation, light irradiation, droplet incubation, droplet reinjection, oxygen delivery, and live/dead assay reagent addition. This multiparametric approach enables information about the efficacy, safety, and effective dosage ranges of PDT agents to be rapidly assayed against target organisms, while also allowing access to data and variables inaccessible using other techniques.

EXPERIMENTAL SECTION

Microfluidic Device Fabrication. The high-throughput microfluidic screening platform consists of three in-line microfluidic modules (Figure 1). The first allows the encapsulation of cells and photosensitizer, toluidine blue O (TBO), in picoliter sized droplets (Figure 1, Device 1). The second allows the incubation and simultaneous irradiation of over 10^5 of these droplets (Figure 1, Device 2), and the third enables on-chip viability scoring of the exposed samples (Figure 1, Device 3). The first and third microfluidic devices were fabricated in PDMS using standard photolithography processes.[33] The second microfluidic device, which contains the incubation chamber (4 mm × 2 mm × 260 μm), was structured in TPE using PDMS as a master mold.[22] The viability-scoring device was fabricated from PDMS and contains an expansion in the microfluidic channel that overlays a pair of chromium−gold electrodes (50 μm electrode width, 30 μm interelectrode spacing) required for droplet fusion. Detailed experimental procedures for device fabrication can be found in the Supporting Information.

Droplet Generation and Collection. *E. coli* (TOP10, Invitrogen, UK) cells were used in all photosensitizer screening experiments. Cells were cultured in Luria−Bertani (LB) broth overnight in a shaking incubator, washed with phosphate buffered saline (PBS, Fisher Scientific, UK) twice, and resuspended in PBS at an optical density of 0.25 (at 600 nm).

Using the first microfluidic device, the *E. coli* suspension and TBO solution were pumped separately into the two aqueous inlets of the device. A standard T-junction was then used to encapsulate the cells and photosensitizer into aqueous droplets within an FC-40 (Fluorinert, 3M, USA) continuous phase containing 1.8% of a custom synthesized biocompatible polyethylene glycol-perfluoropolyether (PEG-PFPE) block copolymer fluorous surfactant to stabilize the droplets over the requisite time scales (see details in the Supporting Information).

dx.doi.org/10.1021/ac4022067 | *Anal. Chem.* 2013, 85, 8866−8872

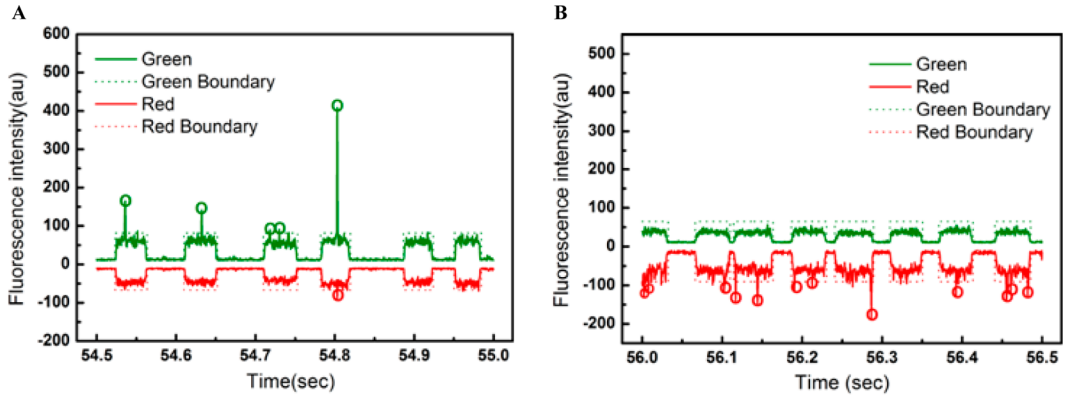

Figure 2. Optical readout of fluorescence traces lasting for 500 ms recorded for (A) live cells and (B) dead cells using the high-throughput microfluidic screening platform. The low-level "rectangular" fluorescence signals correspond to droplet fluorescence signatures, while the narrower, higher intensity peaks report the transit of droplet-encapsulated cells through the detection probe volume.

All solutions were filtered (0.2 μm sterile filters, Pall Corporation, UK) prior to use and pumped into the microfluidic device using 2.5 mL glass gastight syringes (SGE Europe, UK). In addition, cell suspensions were constantly stirred in the syringe using a mini portable magnetic stirrer (Utah Biodiesel Supply, USA). Volumetric flow rates of 5 μL/min and 10 μL/min were used for both the aqueous solutions and the oil phase, respectively, generating 140 pL droplets at approximately 650 Hz. Once formed, droplets were transferred from the generation device into the TPE microfluidic chamber (Device 2) using polytetrafluoroethylene (PTFE) tubing (Smiths Medical International, UK). Transfer was performed over 15 min to allow the collection of approximately 500,000 droplets.

Droplet Incubation and Exposure to Light. The collected droplets were incubated within the TPE chamber (Device 2) and subjected to different exposure conditions, with incubation time scales ranging from several hours up to several days. TBO has an absorbance maximum at approximately 635 nm. Since TPE transmits over 80% of light between 400 and 800 nm,[22] the chamber is highly compatible with the use of TBO as a photosensitizing agent. It is also suitable for screening the majority of photosensitizers used in PDT because most absorb in the red part of the visible spectrum.[40]

After incubation of droplets at 37 °C for 1 h in the dark, droplets were exposed to bright white light ($P \sim 177$ mW/cm^2, tungsten filament transmission light, Olympus, UK). During light irradiation, it was necessary to continuously perfuse oxygenated FC-40 with 1.8% surfactant through the chamber (10 μL/min flow rate) to provide a continuous supply of oxygen for the photosensitization reaction. To ensure that the droplets remained within the microfluidic chamber during this step, the device was tilted by 7° by elevating one side of the device. FC-40 has a high maximum oxygen dissolution content (15 mM compared to 2.2 mM for water[41]) and has been shown to allow rapid oxygen exchange between the oil phase and aqueous droplets in microfluidic systems.[42] Therefore, in the current application, it serves as an ideal continuous phase for delivering the oxygen needed for the photodynamic activation of *E. coli*. In addition, prior to use, the FC-40 (containing 1.8% surfactant) was sparged with oxygen for 1 h. Once oxygenated, the oil was used immediately by dosing from a gastight syringe through polyether ether ketone (PEEK) tubing (1/16 in. outer and 200 μm inner diameter, VWR International, UK). A needle tip (23G, BD, UK) was used to connect the PEEK tubing from the syringe to the PTFE tubing fitted to the TPE chamber, and the connection was made tight using a half block PEEK union (VWR International, UK) to prevent leakage.

Droplet-Based Viability Assays. After incubation within the TPE chamber and exposure to light, droplets were injected into the third microfluidic device for viability scoring. The viability assay agents consisted of 6-carboxyfluorescein diacetate (CFDA, 2 μM, Invitrogen, UK), propidium iodide (PI, 4 μM, Invitrogen, UK), and glutaraldehyde (GTA, 1 g/L, Sigma-Aldrich, UK). CFDA and PI were used to discriminate between live and dead *E. coli* cells. CFDA is a green fluorescent substrate that indicates cell viability by membrane permeation and measurement of enzymatic activity, and PI is a membrane-impermeant red fluorescent nucleic acid dye that labels cells with compromised membranes, i.e., dead cells.[43] Glutaraldehyde was added to the mixture to increase the sensitivity of the live cell signal by preventing the leakage of carboxyfluorescein from the cell (Figure S2, Supporting Information).[44] The viability-scoring device consists of four main components: (1) Reinjection (Figure 1C): The photosensitized, cell-containing droplets were reinjected into the microfluidic device via a reinjection nozzle at a flow rate of 0.4 μL/min. An additional injection of oil through two side channels at 2 μL/min was used to increase the spacing between adjacent droplets. (2) Addition of viability assay agents (Figure 1D,E): A second flow-focusing junction was used to form droplets containing all necessary viability agents. Both the viability agent solution and the oil phase were motivated at a flow rate of 1 μL/min to generate 1.5 nL microdroplets (at a rate of between 10 and 20 Hz). Droplets containing cell suspensions were then merged "one-to-one" with those containing viability assay agents using active electrofusion (7 V square-shaped AC electric field at 1 kHz). (3) Droplet incubation (Figure 1F): Fused droplets were then incubated within a delay line consisting of an expanded channel (1000 μm wide, 260 μm deep, and 31 cm long) to reduce back-pressure. This yielded an approximate incubation time of 25 min for a total flow rate of 4 μL/min and allowed the assay to fully develop on-chip. Although wide channels can induce droplet residence time distributions, this was minimized by operation at higher droplet volume fractions. (4) Droplet detection (Figure 1G): After incubation, the droplets traveled through a fluorescence detection zone having a shallower channel depth (~50 μm). This change in channel cross-section allows efficient optical detection by ensuring that entire droplets pass through the confocal probe volume. Confocal

dx.doi.org/10.1021/ac4022067 | *Anal. Chem.* 2013, 85, 8866−8872

fluorescence microscopy was performed using a custom-built confocal spectrometer capable of resolving single fluorophore events at frequencies in excess of 50 kHz. Briefly, this consists of two avalanche photodiode detectors coupled and a 488 nm laser excitation source. Details of this system are provided in Figure S3 and associated text in the Supporting Information.

In order to assess the performance of the viability assay, dead *E. coli* cell suspensions were prepared by treating the cells with methanol at −20 °C for 10 min. The suspensions were standardized by matching the optical density of both live and dead *E. coli* samples at 600 nm to 0.25. This corresponds to approximately 5×10^7 cells/mL and allowed the preparation of a series of mixtures of dead and live *E. coli* cell solutions with known composition ratios. The viability assay was then performed with these mixtures in both a 96-microwell plate (BD, UK) and a plate reader (Gemini XPS Fluorescence Microplate Reader, Molecular Devices, UK) and in the high-throughput microfluidic screening platform using the custom-built confocal spectrometer.

RESULTS AND DISCUSSION

Calibration of the Microfluidic Platform. Initially, the CFDA/PI assay used to discriminate between live and dead *E. coli* cells was assessed using the high-throughput microfluidic screening assay (Figure 2). Representative examples of time-integrated fluorescence traces over periods of 500 ms are shown in Figure 2. Significantly, the LB medium acts as a weakly fluorescing background defining the aqueous droplet boundaries, with distinct photon bursts corresponding to the presence of individual cells, being distinguishable on top of this background signal. Such fluorescence traces clearly demonstrate that only live cells yield green fluorescence bursts (Figure 2A), while dead cells exhibit only red fluorescence bursts (Figure 2B).

Microbial viability scoring can be difficult to perform within microfluidic devices since bacterial cells are between 5 and 10 times smaller than mammalian cells and therefore generally exhibit weaker fluorescence signals.[44] Accordingly, as a second step toward performing high-throughput photosensitizer screening, we assessed the performance of the viability assay in both a microtiter plate and a droplet-based microfluidic format using mixtures of dead and live *E. coli* cells at known population ratios (Figure 3). The data in Figure 3 exhibit a linear variation of red/green fluorescence ratio as a function of

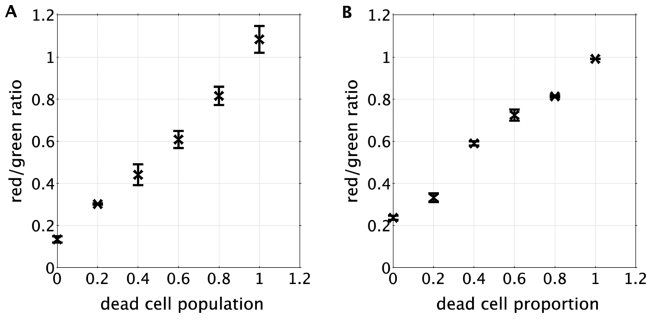

Figure 3. Viability assay performance for *E. coli* cells in (A) a 96-microwell plate and (B) the high-throughput microfluidic screening platform. The assay was performed using preprepared mixtures of dead and live *E. coli* cells at known ratios. For the droplet-based measurements, these solutions were then introduced into the microfluidic platform and cell viability was measured online.

deal cell percentage, with R^2 values of 0.99 and 0.98 for A and B, respectively. However, the *y*-intercept of the trendline (0.23 for the microtiter plate and 0.10 for the microfluidic platform) differs due to the higher death rates associated with cells in the microfluidic device as a result of larger shear forces.[10] Both the microtiter plate and the microdroplet assays show an approximately linear increase in the red/green signal ratio with increasing initial dead cell percentage, which is in accordance with the fact that the "red signal" only reports dead cell concentrations. In addition, the assay exhibits a high degree of specificity with only 1.9% of the dead cells and 9.9% of the live cells showing dual staining

The biocompatibility of the microfluidic system to *E. coli* cells was then assessed, with particular regard to the oil/surfactant mixture and the TPE substrate, since the biocompatibility of PDMS with *E. coli* cells has been well characterized in previous studies.[45] To test the biocompatibility of the oil/surfactant mixture, *E. coli* cells were kept off-chip in aqueous droplets within a surfactant containing oil for periods of at least 5 days. This was followed by performance of the off-chip viability assay. Since the formed droplets were highly stabilized by the surfactant, the emulsion was broken by resuspending the droplets in surfactant-free FC-40 and centrifuging the suspension at 1000 rpm for 5 min. The cell suspensions were then treated with the viability agents (off-chip) and introduced into the microfluidic assay chip for analysis (within droplets) as described previously. Approximately 20% of cells within a "live" cell population were scored as dead after 5 days (Figure 4A). This value is in good agreement with previous reports on cell viability in microdroplets.[46] Importantly, repeat measurements indicated that cell survival rates were consistently above 80%. The cytotoxicity of the thermoset polyester material was also examined. For this, the *E. coli* cell suspensions were incubated within the TPE microfluidic chamber device for a period of up to 4 days. The cell survival rates within the TPE device were also observed to be consistently over 80% during the observation period (Figure 4B). These data show that the materials used in the current microfluidic platform meet the biocompatibility requirements for performing high-throughput screening experiments over extended time periods.

To investigate whether screening within microdroplets had a significant effect on the photodynamic inactivation of *E. coli* cells, microdroplets generated as described above and containing both cells and TBO (1 μM) were exposed to varying doses of electromagnetic radiation in a 96-microwell plate. The emulsion was then broken by centrifugation in surfactant-free FC-40, and the resulting cell suspension was treated with the viability assay agents. Fluorescence-based analysis results were then compared with equivalent bulk experiments under the same conditions, where 100 μL solutions containing cells and TBO (1 μM) were exposed to varying light doses in a 96-microwell plate. Results are illustrated in Figure 5 and demonstrate an approximately linear dependence of cell death with increasing light dose and a strong correspondence between nondroplet and droplet-based exposure methods. Indeed, approximately 50% of cells are dead at a light dose of 315 J/cm^2 for bulk experiments and 313 J/cm^2 for droplet-based experiments (Figure 5A).

High-Throughput Microfluidic Cytotoxicity Screening. The viability of *E. coli* cells when treated with different concentrations of TBO was assessed using the integrated high-throughput photosensitizer-screening platform. First, droplets

dx.doi.org/10.1021/ac4022067 | Anal. Chem. 2013, 85, 8866−8872

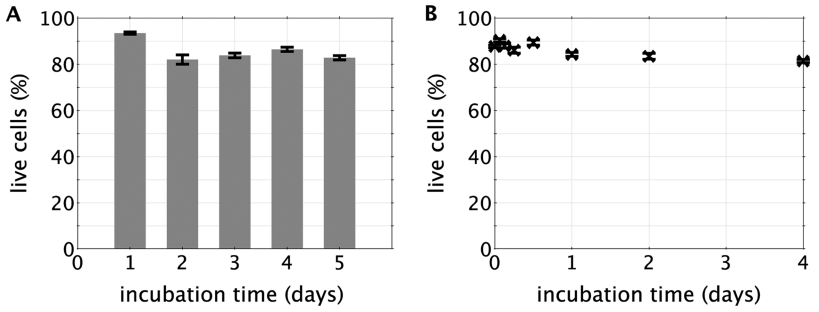

Figure 4. Biocompatibility of microfluidic components with *E. coli* cells. (A) Cell survival time in aqueous droplets within an FC-40 oil phase containing 1.8% perfluorinated surfactant. Cell viability in microdroplets remained over 80% over the course of 5 days. Samples were prepared off-chip and introduced into the microfluidic device for analysis. (B) *E. coli* cell viability within the TPE microfluidic chamber device. Cell viability remains over 80% over the course of 4 days. These data were gathered using SYTO-9 as the assaying agent (see the Supporting Information for details).

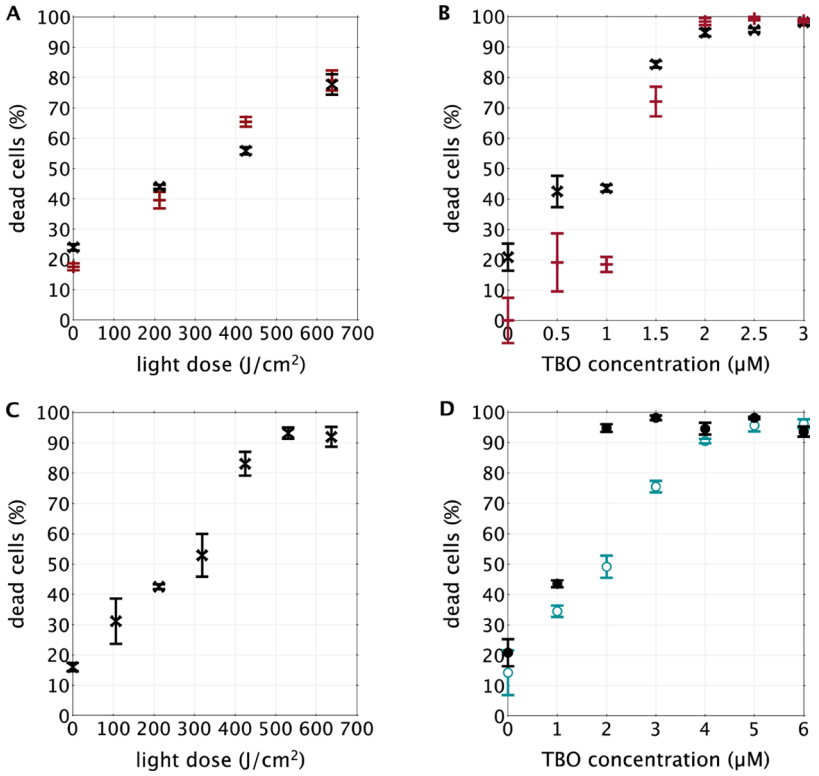

Figure 5. Characterization and control experiments for the high-throughput microfluidic screening platform. (A) Comparison of the effect different light doses and a constant amount of TBO (1 μM) on cell death in bulk on a 96-well plate (+) and in droplets (×). The droplets were created on-chip but put into 96-well plates for light irradiation and treatment with viability assay agents. (B) Comparison of the effect of a light dose of 212.4 J/cm^2 on bulk (CFU assay, +) and microfluidic (×) measurements of cell death with different concentrations of TBO. Both screening methods show similar trends and IC_{50} values. (C) Effect of light dose on cell death as detected on the high-throughput microfluidic screening platform in droplets. The concentration of TBO was kept constant at 1 μM. (D) The effect of TBO concentration at a light dose of 212.4 J/cm^2 with (●) and without (o) perfusion of oxygenated oil through the microfluidic storage. Significantly different dose–response curves and IC_{50} values were generated. Note that the data shown by the black circle (●) in this graph are the same as those shown by the black cross (×) in graph (B).

with a volume of 140 pL containing cells and photosensitizer were created at a rate of 650 droplets per second and collected in the TPE microfluidic chamber. Each droplet contained on average 20 *E. coli* cells, as determined by both traditional colony forming unit (CFU) counting methods and fluorescence imaging of droplets. Droplets were then incubated for 1 h in the dark within the TPE chamber to allow for TBO uptake into the cells prior to light exposure. Light exposed droplets were subsequently injected into the viability-scoring chip. To properly assess the robustness of this high-throughput screening platform, the microfluidic dose–response curve was compared to results obtained from bulk 96-well plate experiments assessed using a conventional CFU assay and associated read-out (Figure 5B). Results indicate a strong correspondence between the CFU and microfluidic-based screening methods. There is a systematic lower limit in the microfluidic platform set by cell death (~20%) inherent in this system. We believe that this is due to shear forces on the cells during the encapsulation process. Each data point in the microfluidic assay data represents an average of 3000 (cell) measurements. Significantly, the microfluidic photosensitizer screening platform shows robust performance with a similar

dx.doi.org/10.1021/ac4022067 | *Anal. Chem.* 2013, 85, 8866–8872

dose response curve to the bulk CFU assay, with an IC_{50} value of 1.1 μM TBO for the microfluidic platform and 1.3 μM TBO for bulk measurements (Figure 6A).

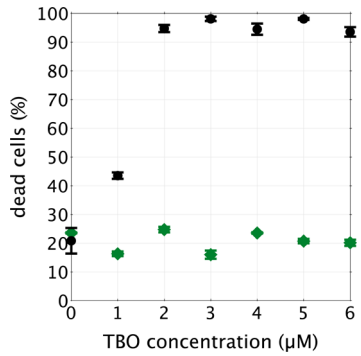

Figure 6. The high-throughput microfluidic screening platform can be used to perform concurrent light and dark toxicity measurements. The experiment was performed at a set light dose, and the effect of TBO was investigated with (●) and without (◆) light exposure. Note that the data shown by the black circle (●) in this graph are the same as that shown by the black circle in Figure 5D.

The effect of light dose on cell viability was also studied using the microfluidic screening platform. As with previous experiments, droplets containing cells and 1 μM TBO were incubated in the dark for an hour but were then exposed to varying light doses within the microfluidic chamber by controlling irradiation time. As the light dose was increased, a concurrent increase in the proportion of dead cells was observed with almost 93% of the cells being dead at doses above 530 J/cm^2 (Figure 5C) and 50% of the cells dead at 250 J/cm^2. Additionally, the effect of perfusing oxygenated oil through the microfluidic chamber during the light irradiation step was investigated (Figure 5D). Without perfusion, cell viability decreased more gradually with TBO concentration than when compared to identical experiments with perfusion of oxygenated oil through the chamber. In fact, almost all cells were dead at 5 μM TBO without perfusion, whereas only 2 μM TBO was required to achieve the same effect when oxygenated oil was perfused through the device during light irradiation. Accordingly, significantly different IC_{50} values (1.94 μM TBO without perfusion and 1.10 μM TBO with oxygenated oil perfusion) were extracted.

Finally, the high-throughput microfluidic screening platform was used to perform concurrent light and dark toxicity measurements on *E. coli* cells at different concentrations of TBO. From Figure 6, it can be seen that 1 μM TBO exhibits no measurable cytotoxicity without light exposure. In fact, no cytotoxic effect of TBO on *E. coli* cells was observed when the droplets containing cells and TBO were incubated for 80 min within the microfluidic chamber under dark conditions, with an average dead cell proportion of approximately 20% across the whole TBO concentration range, as expected (Figure 6).

CONCLUSIONS

We have developed a highly efficient and versatile screening platform for antimicrobial photodynamic therapy agents with a fast and sensitive read-out mechanism. Fluidic modules for droplet generation, prolonged incubation, light irradiation, molecular oxygen delivery, dosing of viability assay agents via droplet merging, and online viability scoring were integrated within a single microfluidic platform. The detection of cell-based fluorescence used in this work allows the live and dead cells to be counted on-chip. The current screening platform operates at a throughput of 10−20 Hz, allowing the screening of hundreds of thousands of separate reaction conditions with an assay volume of 1.5 nL per droplet and a total volume of 4.5 μL per assay point. Calibration of the microfluidic platform demonstrated excellent correspondence with low-throughput assay data obtained using traditional microplate methods. Importantly, the presented platform allows assay data to be recovered in an automated and rapid fashion (~2 h), whereas conventional CFU methods are labor intensive and typically require experiments lasting in excess of 18 h. Perhaps the most interesting feature of the described platform is the ability to directly and concurrently measure the effect of oxygen saturation and dark toxicity in the same device, an operation not possible using CFU counting methods. Indeed, it is also noteworthy that, although each individual measurement is performed on a single cell, the total number of cells assessed provides a statistically significant population measurement, thus highlighting the advantage of single cell measurements coupled with the robustness of population-based measurements.

In conclusion, our droplet-based photosensitizer screening platform is a versatile tool for not only screening various photosensitizers against microbial organisms but also providing valuable multidimensional information such as photosensitizer concentration, light dose, oxygen content, and dark toxicity, which are useful for both medical therapeutic purposes and the fundamental understanding of photobiological processes. Current experiments in our laboratory are assessing use of the described platform to screen libraries of small molecule sensitizers based on phenothiazinium derivatives[47] and the inclusion of cell sorting into this microfluidic platform.

ASSOCIATED CONTENT

Supporting Information

Microfluidic device fabrication methods, synthesis of fluorous surfactant, details regarding the confocal fluorescence spectrometer, viability scoring assay, and CFU assay methods with SYTO-9 and figures regarding the mechanism of action of PDT agents, the effect of GTA on assay sensitivity, and the layout of the confocal fluorescence spectrometer. This material is available free of charge via the Internet at http://pubs.acs.org.

AUTHOR INFORMATION

Corresponding Authors

*E-mail: andrew.demello@chem.ethz.ch. Telephone: +41 44 63 36610.

*E-mail: katherine.elvira@chem.ethz.ch. Telephone: +41 44 633 94 68.

Notes

The authors declare no competing financial interest.

ACKNOWLEDGMENTS

We acknowledge Mark Draper for electrode fabrication, Robert Jarvis for the initial work, and Professor Mark Wainwright for providing sensitizers and valuable advice. This work was partially supported by the National Research Foundation of Korea (Global Research Laboratory Programme Grant K20904000004-10A0500-00410).

REFERENCES

(1) Maisch, T. *Lasers Surg. Med.* **2007**, *22*, 83−91.

(2) Jori, G.; Fabris, C.; Soncin, M.; Ferro, S.; Coppellotti, O.; Dei, D.; Fantetti, L.; Chiti, G.; Roncucci, G. *Lasers Surg. Med.* **2006**, *38*, 468−481.
(3) Wainwright, M. *J. Antimicrob. Chemother.* **1998**, *42*, 13−28.
(4) Wainwright, M. *J. Antimicrob. Chemother.* **2012**, *67*, 787−788.
(5) Hamblin, M. R.; Hasan, T. *Photochem. Photobiol. Sci.* **2004**, *3*, 436−450.
(6) Elvira, K. S.; Wootton, R. C. R.; Reis, N. M.; Mackley, M. R.; deMello, A. J. *ACS Sustainable Chem. Eng.* **2013**, *1*, 209−213.
(7) Nichols, M. G.; Foster, T. H. *Phys. Med. Biol.* **1994**, *39*, 2161.
(8) Maisch, T.; Baier, J.; Franz, B.; Maier, M.; Landthaler, M.; Szeimies, R.-M.; Bäumler, W. *Proc. Natl. Acad. Sci. U. S. A.* **2007**, *104*, 7223−7228.
(9) Wainwright, M. *Dyes Pigm.* **2007**, *73*, 7−12.
(10) Brouzes, E.; Medkova, M.; Savenelli, N.; Marran, D.; Twardowski, M.; Hutchison, J. B.; Rothberg, J. M.; Link, D. R.; Perrimon, N.; Samuels, M. L. *Proc. Natl. Acad. Sci. U. S. A.* **2009**, *106*, 14195−14200.
(11) Boedicker, J. Q.; Li, L.; Kline, T. R.; Ismagilov, R. F. *Lab Chip* **2008**, *8*, 1265−1272.
(12) Guo, M. T.; Rotem, A.; Heyman, J. A.; Weitz, D. A. *Lab Chip* **2012**, *12*, 2146−2155.
(13) Churski, K.; Kaminski, T. S.; Jakiela, S.; Kamysz, W.; Baranska-Rybak, W.; Weibel, D. B.; Garstecki, P. *Lab Chip* **2012**, *12*, 1629−1637.
(14) Theberge, A. B.; Courtois, F.; Schaerli, Y.; Fischlechner, M.; Abel, C.; Hollfelder, F.; Huck, W. T. S. *Angew. Chem., Int. Ed.* **2010**, *49*, 5846−5868.
(15) The, S. Y.; Lin, R.; Hung, L. H.; Lee, A. P. *Lab Chip* **2008**, *8*, 198−220.
(16) Song, H.; Chen, D. L.; Ismagilov, R. F. *Angew. Chem., Int. Ed.* **2006**, *45*, 7336−7356.
(17) Niu, X.; Gulati, S.; Edel, J. B.; deMello, A. J. *Lab Chip* **2008**, *8*, 1837−1841.
(18) Ahn, K.; Agresti, J.; Chong, H.; Marquez, M.; Weitz, D. A. *Appl. Phys. Lett.* **2006**, *88*, 264105.
(19) Link, D. R.; Gransland-Mongrain, E.; Duri, A.; Sarrazin, F.; Cheng, Z.; Cristobal, G.; Marquez, M.; Weitz, D. A. *Angew. Chem., Int. Ed.* **2006**, *45*, 2556−2560.
(20) Chabert, M.; Dorfman, K. D.; Viovy, J. L. *Electrophoresis* **2005**, *26*, 3706−3715.
(21) Niu, X.; Gielen, F.; deMello, A. J.; Edel, J. B. *Anal. Chem.* **2009**, *81*, 7321−7325.
(22) Kim, J. Y.; deMello, A. J.; Chang, S. I.; Hong, J.; O'Hare, D. *Lab Chip* **2011**, *11*, 4108−4112.
(23) Draper, M. C.; Niu, X.; Cho, S.; James, D. I.; Edel, J. B. *Anal. Chem.* **2012**, *84*, 5801−5808.
(24) Tice, J. D.; Song, H.; Lyon, A. D.; Ismagilov, R. F. *Langmuir* **2003**, *19*, 9127−9133.
(25) Solvas, X. C.; Srisa-Art, M.; deMello, A. J.; Edel, J. B. *Anal. Chem.* **2010**, *82*, 3950−3956.
(26) Abate, A. R.; Hung, T.; Mary, P.; Agresti, J. J.; Weitz, D. A. *Proc. Natl. Acad. Sci. U. S. A.* **2010**, *105*, 3191−3196.
(27) Frenz, L.; Blank, K.; Brouzes, E.; Griffiths, A. D. *Lab Chip* **2008**, *9*, 1344−1348.
(28) Hatch, A. C.; Fisher, J. S.; Tovar, A. R.; Hsieh, A. T.; Lin, R.; Pentoney, S. L.; Yang, D. L.; Lee, A. P. *Lab Chip* **2011**, *11*, 3838−3845.
(29) Ahn, K.; Kerbage, C.; Hunt, T. P.; Westervelt, R. M.; Link, D. R.; Weitz, D. A. *Appl. Phys. Lett.* **2006**, *88*, 024104.
(30) Baret, J. C.; Ryckelynck, M.; El-Harrak, A.; Frenz, L.; Rick, C.; Samuels, M. L.; Hutchison, J. B.; Agresti, J. J.; Link, D. R.; Weitz, D. A.; Griffiths, A. D. *Lab Chip* **2009**, *9*, 1850−1858.
(31) Abate, A. R.; Agresti, J. J.; Weitz, D. A. *Appl. Phys. Lett.* **2010**, *96*, 203509.
(32) Niu, X.; Gielen, F.; Edel, J. B.; deMello, A. J. *Nat. Chem.* **2011**, *3*, 437−442.
(33) Duffy, D. C.; McDonald, J. C.; Schueller, O. J. A.; Whitesides, G. M. *Anal. Chem.* **1998**, *70*, 4974−4984.
(34) Bu, M. Q.; Melvin, T.; Ensell, G. J.; Wilkinson, J. S.; Evans, A. G. R. *Sens. Actuators, A* **2004**, *115*, 476−482.
(35) Qin, D.; Xia, Y. N.; Rogers, J. A.; Jackman, R. J.; Zhao, X. M.; Whitesides, G. M. *Microsyst. Technol. Chem. Life Sci.* **1998**, *194*, 1−20.
(36) Choi, J.-W.; Kang, D.-K.; Park, H.; deMello, A. J.; Chang, S.-I. *Anal. Chem.* **2012**, *84*, 3849−3854.
(37) Agresti, J. J.; Antipov, E.; Abate, A. R.; Ahn, K.; Rowat, A. C.; Baret, J. C.; Marquez, M.; Klibanov, A. M.; Griffiths, A. D.; Weitz, D. A. *Proc. Natl. Acad. Sci. U. S. A.* **2010**, *107*, 4004−4009.
(38) Debs, B. E.; Utharala, R.; Balyasnikova, I. V.; Griffiths, A. D.; Merten, C. A. *Proc. Natl. Acad. Sci. U. S. A.* **2012**, *109*, 11570−11575.
(39) Leung, K.; Zahn, H.; Leaver, T.; Konwar, K. M.; Hanson, N. W.; Pagé, A. P.; Lo, C.-C.; Chain, P. S.; Hallam, S. J.; Hansen, C. L. *Proc. Natl. Acad. Sci. U. S. A.* **2012**, *109*, 7665−7670.
(40) Sternberg, E. D.; Dolphin, D.; Bruckner, C. *Tetrahedron* **1998**, *54*, 4151−4202.
(41) Ntwampe, S. K. O.; Williams, C. C.; Sheldon, M. S. *Afr. J. Biotechnol.* **2010**, *9*, 1106−1114.
(42) Abbyad, P.; Tharaux, P.-L.; Martin, J.-L.; Baroud, C. N.; Alexandrou, A. *Lab Chip* **2010**, *10*, 2505−2512.
(43) Kaneshiro, E. S.; Wyder, M. A.; Wu, Y.-P.; Cushion, M. T. *J. Microbiol. Methods* **1993**, *17*, 1−16.
(44) Miyanaga, K.; Takano, S.; Morono, Y.; Hori, K.; Unno, H.; Tanji, Y. *Biochem. Eng. J.* **2007**, *37*, 56−61.
(45) Long, Z.; Nugent, E.; Javer, A.; Cicuta, P.; Sclavi, B.; Cosentino Lagomarsino, M.; Dorfman, K. D. *Lab Chip* **2013**, *13*, 947−954.
(46) Clausell-Tormos, J.; Lieber, D.; Baret, J. C.; El-Harrak, A.; Miller, O. J.; Frenz, L.; Blouwolff, J.; Humphry, K. J.; Koster, S.; Duan, H.; Holtze, C.; Weitz, D. A.; Griffiths, A. D.; Merten, C. A. *Chem. Biol.* **2008**, *15*, 427−437.
(47) Wainwright, M.; Smalley, H.; Scully, O.; Lotfipour, E. *Photochem. Photobiol.* **2012**, *88*, 523−526.